

# UC Irvine

## UC Irvine Previously Published Works

### Title

Greenhouse gas emissions from diverse Arctic Alaskan lakes are dominated by young carbon

### Permalink

<https://escholarship.org/uc/item/9q0086pg>

### Journal

Nature Climate Change, 8(2)

### ISSN

1758-678X

### Authors

Elder, CD  
Xu, X  
Walker, J  
et al.

### Publication Date

2018-02-01

### DOI

10.1038/s41558-017-0066-9

Peer reviewed

# Greenhouse gas emissions from diverse Arctic Alaskan lakes are dominated by young carbon

Clayton D. Elder<sup>1\*</sup>, Xiaomei Xu<sup>1</sup>, Jennifer Walker<sup>1</sup>, Jordan L. Schnell<sup>1,7</sup>, Kenneth M. Hinkel<sup>2,8</sup>, Amy Townsend-Small<sup>3</sup>, Christopher D. Arp<sup>4</sup>, John W. Pohlman<sup>5</sup>, Benjamin V. Gaglioti<sup>6</sup> and Claudia I. Czimczik<sup>1\*</sup>

**Climate-sensitive Arctic lakes have been identified as conduits for ancient permafrost-carbon (C) emissions and as such accelerate warming. However, the environmental factors that control emission pathways and their sources are unclear; this complicates upscaling, forecasting and climate-impact-assessment efforts. Here we show that current whole-lake CH<sub>4</sub> and CO<sub>2</sub> emissions from widespread lakes in Arctic Alaska primarily originate from organic matter fixed within the past 3–4 millennia (modern to 3,300 ± 70 years before the present), and not from Pleistocene permafrost C. Furthermore, almost 100% of the annual diffusive C flux is emitted as CO<sub>2</sub>. Although the lakes mostly processed younger C (89 ± 3% of total C emissions), minor contributions from ancient C sources were two times greater in fine-textured versus coarse-textured Pleistocene sediments, which emphasizes the importance of the underlying geological substrate in current and future emissions. This spatially extensive survey considered the environmental and temporal variability necessary to monitor and forecast the fate of ancient permafrost C as Arctic warming progresses.**

Lakes are more abundant in the Arctic than in any other region<sup>1</sup> and emit more CH<sub>4</sub> than any other natural Arctic source, contributing 6% (16.5 Tg CH<sub>4</sub> yr<sup>-1</sup>) to global natural CH<sub>4</sub> emissions<sup>2,3</sup>. Current CH<sub>4</sub> emission estimates from Arctic lakes vary by a factor of two (11.9–24.2 Tg CH<sub>4</sub> yr<sup>-1</sup>) (refs <sup>4–6</sup>), and future estimates from all permafrost-region sources span three orders of magnitude<sup>7</sup>. Discrepancies persist because of uncertain climate projections<sup>8</sup> and because current lake-C-emission data sets fail to capture the complexity of Arctic-lake types<sup>9</sup>, specifically, their geological settings<sup>10</sup>, potential C sources<sup>11,12</sup> and CH<sub>4</sub> versus CO<sub>2</sub> emission pathways<sup>13,14</sup>.

Approximately 20% of the total lake area in northern permafrost regions formed via thermokarst, in which degradation of ice-rich permafrost results in subsidence, ponding and thaw of the underlying sediments<sup>11</sup>. The initiation and expansion of thermokarst lakes is sensitive to climate change<sup>15</sup>, and has been identified as a mechanism for the rapid decomposition of ancient (defined here as ≥ 11,500 years before the present (YBP), that is, late Pleistocene and older) permafrost C and its emission to the atmosphere<sup>16–18</sup>. Under a warming climate, there is the potential for an enhanced decomposition and emission of this ancient and vast C reservoir to provide a positive feedback to climate change<sup>14</sup>. Yet, the ability of thermokarst lakes to act as conduits for permafrost C emissions to the atmosphere as CH<sub>4</sub> has only been verified in lakes that actively thaw into yedoma, a fine-textured, C- and ice-rich, aeolian sediment of the Pleistocene steppe. These environmental conditions comprise just 12% (150,000 km<sup>2</sup>) of the landscapes with prevalent lake thermokarst (1,300,000 km<sup>2</sup>) in the northern circumpolar permafrost region (18,410,000 km<sup>2</sup>) (refs <sup>10,11</sup>), and therefore under-represent the environmental diversity of Arctic lakes.

Current estimates of permafrost C loss from lakes are based on age measurements (radiocarbon (<sup>14</sup>C) dating) of CH<sub>4</sub> emitted by ebullition (bubbling). Measured ages are highly variable, ranging from 40,000 YBP to modern (C fixed from the atmosphere after 1950) within a single lake<sup>16,17,19,21</sup>. Ebullition itself is highly sporadic, and daily rates can span three orders of magnitude<sup>13,22–24</sup>. And, although ebullition is probably the primary CH<sub>4</sub> emission pathway in actively expanding yedoma–thermokarst lakes (79% of the total emissions on average)<sup>2,18</sup>, diffusive CH<sub>4</sub> emissions can dominate whole-lake emissions in non-yedoma systems<sup>13,25</sup>. Furthermore, northern lakes can also be large CO<sub>2</sub> sources<sup>26</sup>, but few studies have simultaneously quantified CH<sub>4</sub> and CO<sub>2</sub> emissions<sup>22,27</sup> or their C-source ages<sup>28</sup>, which leaves an incomplete understanding of the role of lakes in the climate feedback of permafrost C.

**Study location and approach.** This study quantified whether ancient permafrost or young organic C (OC) dominates whole-lake C emissions from lakes on Alaska's North Slope, and the proportion emitted as CH<sub>4</sub>. In our 250,000 km<sup>2</sup> study region, lakes are a dominant landscape feature<sup>29</sup>, formed by a variety of processes, which include thermokarst, in a diverse range of geological substrates<sup>9</sup>. Most of the North Slope remained unglaciated during the most-recent glacial maximum (~27–19 kyr ago) and has accumulated sediments with varying OC<sup>30</sup> and ice content<sup>31</sup>. The general surficial geology is delineated by mixtures of marine gravel, sand, silt and clay (coastal-plain geology), glaciomarine deposits near the Beaufort and Chukchi Sea coasts<sup>32</sup>, a 250 × 60 km<sup>2</sup> zone of aeolian sand further inland<sup>33</sup>, yedoma-type aeolian silt along the northern edge of the Brooks range<sup>34</sup> and rivers that flow south to north with floodplain corridors underlain by fluvial sand and glacial outwash (Supplementary Fig. 1).

<sup>1</sup>Department of Earth System Science, University of California, Irvine, CA, USA. <sup>2</sup>Department of Geography, University of Cincinnati, Cincinnati, OH, USA. <sup>3</sup>Department of Geology, University of Cincinnati, Cincinnati, OH, USA. <sup>4</sup>Water and Environmental Research Center, University of Alaska, Fairbanks, AK, USA. <sup>5</sup>USGS Woods Hole Coastal and Marine Science Center, Woods Hole, MA, USA. <sup>6</sup>Lamont-Doherty Earth Observatory of Columbia University, Palisades, NY, USA. Present addresses: <sup>7</sup>Department of Earth and Planetary Sciences, Northwestern University, Evanston, IL, USA. <sup>8</sup>Geological and Mining Engineering and Sciences, Michigan Technological University, Houghton, MI, USA. \*e-mail: [cdelder@uci.edu](mailto:cdelder@uci.edu); [czimczik@uci.edu](mailto:czimczik@uci.edu)

We quantified the  $^{14}\text{C}$  age,  $^{13}\text{C}$  content and concentrations of mass-integrated, whole-lake diffusive  $\text{CH}_4$  and  $\text{CO}_2$  in up to 40 lakes that span seven geological sediment types<sup>35</sup>, thermokarst and non-thermokarst lake types, and a  $3.5^\circ\text{C}$  gradient in mean annual air temperature (Supplementary Table 1). The 40 lakes were studied over two winters (April 2013 and April 2014), and seven were studied during one summer (August 2014). Isotope measurements were made on  $\text{CH}_4$  and  $\text{CO}_2$  dissolved beneath floating ice in late winter, when the majority of any ebullition gas, trapped beneath the ice, would have dissolved into the lake water over the ice-cover season<sup>36</sup>. We assume that the  $^{14}\text{C}$  signature of dissolved ebullition gas would alter the whole-lake dissolved  $^{14}\text{C}$  signature by the principle of mass balance (see equation (8)), and that the below-ice  $^{14}\text{C}$  signature of dissolved gases represents the mass-integrated value of the whole-lake emissions. Cumulative daily C fluxes for the open-water period were estimated by extrapolating the mean of triplicate dissolved  $\text{CH}_4$  and  $\text{CO}_2$  measurements, made on either a single day ( $n=7$ ) or on two days (one week apart) ( $n=2$ ) in August 2014, using daily air and water temperature, and daily wind speed. Annual diffusive emissions (g C) of  $\text{CH}_4$  and  $\text{CO}_2$  were estimated for each lake surveyed in the summer by adding an estimate of the springtime ice-out diffusive flux (based on below-ice accumulation) to cumulative daily fluxes from the ice-free period (Table 1 (Methods)).

We estimated the mean and probable range of ancient permafrost C contributions to the whole-lake emissions of  $\text{CH}_4$  and  $\text{CO}_2$  with a five-source isotope mass-balance model<sup>37</sup>. Carbon-source categories included C fixed from the atmosphere during 1950–2012 (which represents  $^{14}\text{C}$ -enriched  $\text{CO}_2$  from nuclear weapons testing), in 2013 (recent photoassimilates), 5,000 YBP (mid-Holocene), 11,500 YBP (end of the Pleistocene) and from  $^{14}\text{C}$ -free sources ( $>50,000$  YBP) (equation (8)).

**Sources of  $\text{CH}_4$  and  $\text{CO}_2$  emissions.** All lakes but one were oversaturated in  $\text{CH}_4$  and  $\text{CO}_2$  ( $n=40$ ) (Fig. 1 and Supplementary Table 2). When an estimate of the ice-out flux is included, we found that all the lakes were sources of C to the atmosphere. Mean daily fluxes were  $6.2 \pm 3.4 \text{ mg CH}_4 \text{ m}^{-2} \text{ d}^{-1}$  and  $2,620 \pm 2,240 \text{ mg CO}_2 \text{ m}^{-2} \text{ d}^{-1}$  ( $n=7$ ), and within the range previously reported from North Slope lakes using similar methods<sup>27</sup>. Total lake-C emissions from the study area were  $0.94 \pm 0.14 \text{ Tg C yr}^{-1}$  (C here is diffusive  $\text{C-CO}_2 + \text{C-CH}_4$ ) (Table 1) and C- $\text{CO}_2$  emissions were over 180 times larger, on average, than C- $\text{CH}_4$  emissions.

Ages of whole-lake diffusive C emissions were much younger (Fig. 2 and Table 1) than the age of  $\text{CH}_4$  emitted from yedoma-thermokarst lakes in Siberia and Central Alaska<sup>16,17</sup> and the age of permafrost C sources ( $>50,000$  to 6,000 YBP)<sup>19</sup>. Ages ranged from modern to  $3,300 \pm 70$  YBP for dissolved  $\text{CH}_4$ , and from modern to  $1,590 \pm 20$  YBP for dissolved  $\text{CO}_2$ . The lake-category-weighted mean  $^{14}\text{C}$  ages for the study region were 847 YBP for  $\text{CH}_4$  ( $n=49$  measurements) and 392 YBP for  $\text{CO}_2$  ( $n=68$ ). In all lakes but one, dissolved  $\text{CH}_4$  was on average 400  $^{14}\text{C}$ -years older than  $\text{CO}_2$  (Fig. 2 and Table 1). This may reflect a combination of modern atmospheric  $\text{CO}_2$  equilibrating with lake waters,  $\text{CO}_2$  production from the aerobic decomposition of younger organic material produced within lakes and imported from surrounding soils, and methanogenesis being fuelled by older sedimentary and soil C sources. Stable isotope data ( $\delta\text{D}$  and  $\delta^{13}\text{C}$  ( $\delta^{13}\text{C} = [({}^{13}\text{C}/{}^{12}\text{C})_{\text{sample}}/({}^{13}\text{C}/{}^{12}\text{C})_{\text{standard}}] - 1$ )) of  $\text{CH}_4$  confirmed a microbial  $\text{CH}_4$  origin in our lakes<sup>38</sup>. In our study, the  $\delta^{13}\text{C}$  of dissolved  $\text{CH}_4$  below ice was  $-56.7 \pm 12.4\text{‰}$  ( $n=16$ ) (Supplementary Table 2), which again indicates microbial  $\text{CH}_4$  ( $\delta^{13}\text{C} < -50\text{‰}$ ) (ref. <sup>39</sup>). The  $^{14}\text{C}$  and  $^{13}\text{C}$  data both demonstrate that lake-C emissions originated primarily from the degradation of recently formed terrestrial C, such as shallow-lake sediment C and

**Table 1 | Diffusive C fluxes and ages from lakes to the atmosphere on the North Slope of Alaska**

Geology type	Total lake area (km <sup>2</sup> )	Below-ice $^{14}\text{C}$ measured ( $n$ lakes ( $\text{CH}_4$ , $\text{CO}_2$ ))	Fluxes measured (August 2014)	Diffusive $\text{CH}_4$ emissions <sup>a</sup> (g $\text{CH}_4 \text{ km}^{-2} \text{ yr}^{-1}$ )	Fraction of $\text{CH}_4$ sourced by ancient C (mean (10th to 90th percentile range))	Mean age of $\text{CH}_4$ emissions (YBP (mean $\pm$ s.d., error if $n=1$ ))	Diffusive $\text{CO}_2$ emissions <sup>a</sup> (g $\text{CO}_2 \text{ km}^{-2} \text{ yr}^{-1}$ )	Fraction of $\text{CO}_2$ sourced by ancient C (mean (10th to 90th percentile range))	Mean age of $\text{CO}_2$ emissions (YBP (mean $\pm$ s.d., error if $n=1$ ))
Glaciomarine	538	1, 2	1	$1.1 \times 10^6$	0.23 (0.0–0.50)	$1,809 \pm 163^b$	$1.1 \times 10^6$	0.17 (0.0–0.38)	$1,029 \pm 626$
Coastal plain	3,383	9, 10	3	$7.9 \times 10^5$	0.21 (0.0–0.45)	$1,560 \pm 478$	$4.1 \times 10^8$	0.15 (0.0–0.35)	$809 \pm 334$
Aeolian silt	483	3, 8	2	$7.5 \times 10^5$	0.19 (0.0–0.45)	$1,280 \pm 473$	$3.8 \times 10^8$	0.15 (0.0–0.35)	$719 \pm 431$
Aeolian Sand	3,028	9, 9	1	$3.2 \times 10^5$	0.11 (0.0–0.25)	$253 \pm 422$	$2.9 \times 10^8$	0.09 (0.0–0.23)	$18 \pm 32$
Glacial young <sup>c</sup>	167	1, 2	n.m.	n.m.	0.08 (0.0–0.25)	$0 \pm 15$	n.m.	0.14 (0.0–0.35)	$603 \pm 884$
Fluvial old <sup>c</sup>	560	1, 1	n.m.	n.m.	0.11 (0.0–0.25)	$97 \pm 25$	n.m.	0.09 (0.0–0.20)	$0 \pm 25$
Fluvial young <sup>c</sup>	506	3, 6	n.m.	n.m.	0.08 (0.0–0.20)	$0 \pm 50$	n.m.	0.10 (0.0–0.25)	$200 \pm 358$
Observed total	8,664	40	7						
North Slope Total <sup>d</sup>	10,659	40	7	$(5.0 \pm 0.8) \times 10^{-3}$ (Tg C- $\text{CH}_4 \text{ yr}^{-1}$ )	$0.14 \pm 0.05$ (flux-weighted (mean $\pm$ s.d.))	$847 \pm 798$ (area-weighted (mean $\pm$ s.d.))	$0.94 \pm 0.16$ (Tg C- $\text{CO}_2 \text{ yr}^{-1}$ )	$0.11 \pm 0.03$ (flux-weighted (mean $\pm$ s.d.))	$392 \pm 495$ (area-weighted (mean $\pm$ s.d.))

<sup>a</sup>Assumes the diffusive flux occurs only during ice-free days (mean = 122 d), incorporates fluctuating water temperatures and wind speeds in 2014, and the additional total mass loss of  $\text{CH}_4$  and  $\text{CO}_2$  during the spring melt (ice-out flux). This estimate does not include potential ice-free ebullition. <sup>b</sup>Error range represents the s.d. of the  $^{14}\text{C}$  age of  $\text{CH}_4$  within one lake measured in both 2013 and 2014.

<sup>c</sup>Where open-water fluxes were not measured (n.m.), annual fluxes were prescribed from other geology category means based on similar below-ice dissolved  $\text{CH}_4$  and  $\text{CO}_2$  concentrations. <sup>d</sup>Extrapolated from the observed lake area of 8,664 (81% of the total lake-area survey).

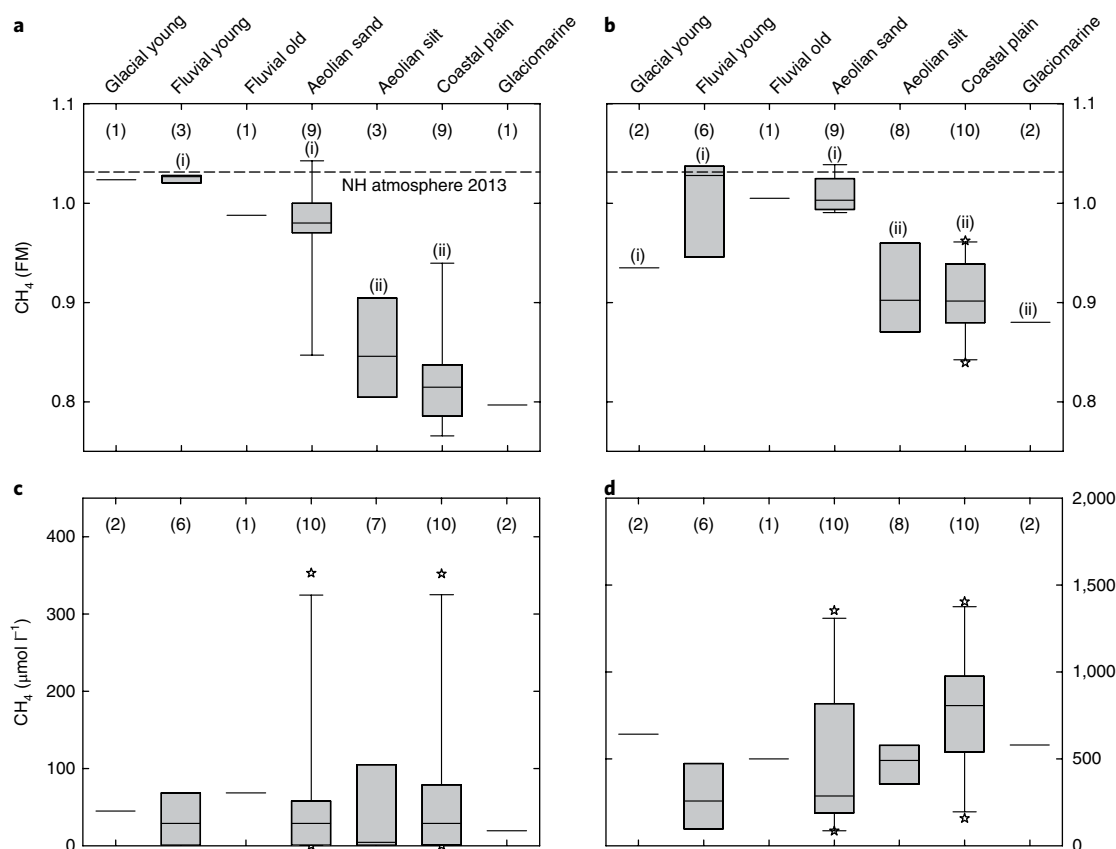


**Fig. 1** |  $^{14}\text{C}$  content and concentration of below-ice dissolved CH $_4$  and CO $_2$  by geological unit. **a–d**, Box plots of lake-dissolved  $^{14}\text{C}$ -CH $_4$  contents (**a**) and  $^{14}\text{C}$ -CO $_2$  contents (**b**), expressed as fraction modern (FM), and dissolved CH $_4$  (**c**) and CO $_2$  (**d**) concentrations in relation to surficial geological unit<sup>36</sup>. Values are averaged from the 2013 and 2014 winter measurements. Dashed horizontal lines indicate the  $^{14}\text{C}$  signature of atmospheric CO $_2$  in the summer of 2013. Boxes indicate the 25th and 75th percentiles, and error bars are the 10th and 90th percentiles. Solid horizontal lines within boxes indicate the median. Open stars are outliers. Numbers within the parentheses indicate the number of lakes observed in each geological unit. Statistically different groups with respect to mean  $^{14}\text{C}$  age are indicated by either (i) or (ii) (single-factor ANOVA and Tukey's HSD post hoc analysis ( $F(4, 21) = 19.49$ ,  $P = 7.92 \times 10^{-7}$ ) and ( $F(4, 30) = 10.85$ ,  $P = 1.46 \times 10^{-5}$ ) for CH $_4$  and CO $_2$ , respectively).

surrounding soil C, rather than fossil C seeping through gaps in the permafrost from near-surface coal beds<sup>40</sup> or from C in sublake thawed sediments (talik) deposited during the Pleistocene<sup>16</sup>.

**Seasonal effects on dissolved CH $_4$  and CO $_2$  isotopes.** Comparing winters within the same lakes, dissolved CH $_4$  was 38% older on average in 2014 than in 2013 ( $p < 0.05$ ,  $n = 12$ ); however, we found no difference in the ages of dissolved CO $_2$  ( $p > 0.05$ ,  $n = 19$ ). Seasonally, the mean age of dissolved CH $_4$  in the winter was 180  $^{14}\text{C}$ -years older than that in the summer ( $p < 0.05$ ,  $n = 6$ ), and the mean age of dissolved CO $_2$  in the winter was 620  $^{14}\text{C}$ -years older than that in the summer ( $p < 0.05$ ,  $n = 6$ ). The older CO $_2$  observed below ice probably reflects a diminished aerobic decomposition of fresh (and young) organic material beneath the ice, and/or limited atmospheric exchange through the ice. We also found strong evidence for the oxidation of CH $_4$  into CO $_2$ , which could also explain the older below-ice CO $_2$  values because CH $_4$  was consistently older than the concomitant CO $_2$ . The mean  $^{14}\text{C}$  values of coexisting dissolved CH $_4$  and CO $_2$  were positively correlated across all the study lakes ( $r = 0.93$ ,  $p < 0.05$ ,  $n = 26$ ) (Fig. 2). This relationship implies CH $_4$  oxidation in the water column, in which the resulting dissolved CO $_2$  carries the  $^{14}\text{C}$  signature of the oxidized CH $_4$ . However, co-production of CH $_4$  and CO $_2$  with the same  $^{14}\text{C}$  signature in sediments during acetate fermentation may also be a factor, especially where coexisting CH $_4$  and CO $_2$  are closer in  $^{14}\text{C}$  age. If we assume that CH $_4$

oxidation is the only factor that alters the  $^{14}\text{C}$  signature of below-ice dissolved CO $_2$ , a two-source  $^{14}\text{C}$  mass-balance mixing model (which utilizes the previous summer  $^{14}\text{CO}_2$  and winter  $^{14}\text{CH}_4$  values as the end members) can be used to estimate that  $60 \pm 15\%$  ( $n = 5$ ) of below-ice dissolved CO $_2$  may have originated from oxidized CH $_4$ . In support of this hypothesis, we found that below-ice dissolved CH $_4$  was enriched in  $^{13}\text{C}$  in six lakes ( $\delta^{13}\text{C}$  ranged from  $-39.5\text{‰}$  to  $-19.0\text{‰}$ ) relative to the common products of methanogenesis ( $\delta^{13}\text{C}$  from  $-110$  to  $-50\text{‰}$ ) (ref. <sup>39</sup>). Likewise, significant negative relationships between below-ice dissolved CH $_4$  concentrations and  $\delta^{13}\text{C}$  in lakes when  $\delta^{13}\text{C} > -60\text{‰}$  were also observed ( $R^2 = 0.59$ ,  $n = 4$  in 2013, and  $R^2 = 0.91$ ,  $n = 7$  in 2014 ( $p < 0.05$ )). Both observations are indicative that CH $_4$  consumption enriches the  $^{13}\text{C}$  in residual dissolved CH $_4$  in a semiclosed system below ice. Together, these findings support our observations that the dissolved C-CO $_2$  pool was four times larger than the C-CH $_4$  pool, that below-ice CH $_4$  oxidation may age the dissolved C-CO $_2$  pool and that within-lake CH $_4$  oxidation regulates the global warming impact of Arctic lakes.

**Emission ages in relation to geological substrate.** The interannual and seasonal variation in mean gas ages for individual lakes was small compared with the age differences observed across geological units (around 160%). Across the North Slope, C-emission ages were clearly related to the surficial geological unit that underlies the lakes (Figs. 1 and 3). Dissolved CH $_4$  and CO $_2$  were significantly younger

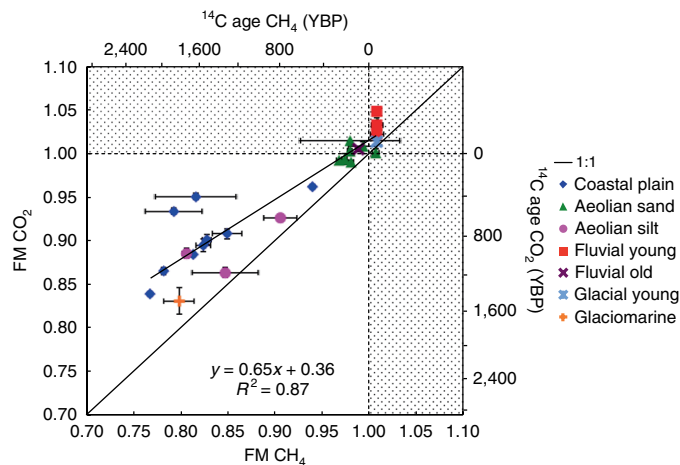


**Fig. 2 | Radiocarbon content of coexisting dissolved  $\text{CH}_4$  and  $\text{CO}_2$  below ice.** Values, expressed as FM and  $^{14}\text{C}$  age (YBP), represent the below-ice mean values from April 2013 and April 2014 ( $n=2$ ) or either the 2013 or 2014 value ( $n=1$ ). Error bars represent the s.d. when  $n=2$ , or the procedural and analytical error when  $n=1$ ; in either case, the larger of the two is shown. Larger errors for  $\text{CH}_4$ , relative to  $\text{CO}_2$ , represent a combination of greater interannual variability and smaller sample size, for which procedural and analytical errors are more impactful. A greater distance from the 1:1 line indicates a greater  $^{14}\text{C}$  content (age) difference between  $\text{CH}_4$  and  $\text{CO}_2$ . Values greater than FM = 1 (shaded area) indicate samples that contain C fixed from the atmosphere post calendar year 1950.

in lakes in sandy and fluvial deposits compared with those in finer-textured coastal, glaciomarine and aeolian silt (yedoma-type) deposits ( $p < 0.05$ , Single factor analysis of variance (ANOVA) and Tukey's honest significant difference (HSD) test and posthoc analysis) (Fig. 1). Mean gas ages in lakes that reside on glacial deposits were not significantly different from gas ages in any other geological unit.

**Sedimentary OC.** The geological substrate incorporates sediment texture, and thus the ground ice content, thermokarst behaviour and C-retention properties of the landscape. In contrast with lakes that form in sandy deposits, lakes in finer, ice-rich sediments exhibit a greater post-thaw subsidence, and thus can quickly degrade deeper (and presumably older) permafrost<sup>9</sup>. Also, as fine-textured Pleistocene aeolian silt on the North Slope sequestered more C, lakes that formed into such deposits have more ancient sedimentary OC available within their taliks for potential decomposition than lakes in sand, given similar thaw depths. We determined that the OC content of aeolian silt ( $0.95 \pm 0.34\%$  OC,  $n=38$ ) was relatively OC rich compared with that of the adjacent aeolian sand ( $0.19 \pm 0.10\%$  OC,  $n=29$ ) ( $p < 0.05$ ) (Supplementary Table 3). This result is similar to previous reports of the North Slope silt<sup>34</sup>, yet less than that of other yedoma-type sediments<sup>10</sup>. The large difference in sedimentary OC observed between sand and silt is also reflected in the five-source isotope model solutions, in which ancient C accounts for an average of 15% of the whole-lake C emissions ( $\text{CH}_4$  plus  $\text{CO}_2$ ) from lakes in silt versus 9% from those in sand (Fig. 4 and Table 1). As finer deposits dominate both ends of our transects, we found no correlation of  $\text{CH}_4$  or  $\text{CO}_2$  age with latitude or mean annual air temperature. Hence, our results demonstrate that local environmental heterogeneity (that is, variable % OC in the substrate) is a better proxy for whole-lake diffusive C-emission ages than is broad climatic regulation on the North Slope.

**Regional  $\text{CH}_4$  and  $\text{CO}_2$  fluxes.** Our regional assessment clearly demonstrates that terrestrial C, fixed from the atmosphere within

the past few millennia, is the dominant source of whole-lake C emissions on the North Slope today, and that the current emissions of ancient C are minimal and restricted to lakes that reside in fine-textured sediments (Figs. 1, 3 and 4). The annual diffusive  $\text{CH}_4$  flux extrapolated from all the lakes (total lake area,  $10,659 \text{ km}^2$ ) in our study region ( $231,157 \text{ km}^2$ ) was  $(5.0 \pm 0.8) \times 10^{-3} \text{ Tg C-CH}_4 \text{ yr}^{-1}$ , of which ancient permafrost C sources contribute a mean of 14%, with a range of 0–38% (10th to 90th percentile range of the mixing-model solutions) (Fig. 4 and Table 1). This is equivalent to an ancient C flux of  $7.2 \times 10^{-4} \text{ Tg C-CH}_4 \text{ yr}^{-1}$  (Table 1). The total annual diffusive  $\text{CO}_2$  emissions were  $0.94 \pm 0.14 \text{ Tg C-CO}_2 \text{ yr}^{-1}$ , with a mean contribution of 11% (range from 0 to 25%) from ancient C (Fig. 4 and Table 1). Ancient C- $\text{CO}_2$  emissions ( $0.10 \text{ Tg C-CO}_2 \text{ yr}^{-1}$ ) were 150 times greater than that via  $\text{CH}_4$ , which implies that  $\text{CO}_2$  diffusion is the dominant pathway for ancient C loss from the North Slope.

**Discussion and conclusion.** Emissions of C to the atmosphere from ancient sources amplify climate warming because they represent a net addition to the active C cycle. Emissions of ancient C were greatest per unit area ( $(1.7 \pm 0.5) \times 10^7 \text{ g C km}^{-2} \text{ yr}^{-1}$ ) and collectively  $((5.7 \pm 2.0) \times 10^{10} \text{ g C yr}^{-1})$  from the lakes in the coastal plain geology unit (Table 1). This is a result of the greater overall lake area (Table 1), a higher proportion of ancient C that contributes to the emissions and a relatively older  $\text{CO}_2$  that accounts for a higher proportion of the total diffusive flux (Table 1). Recent work suggests that increasing winter water temperatures are preventing lakes in this region from freezing completely in the winter<sup>15</sup>, which potentially allows aged organic material in newly developing taliks to contribute to greenhouse-gas production.

The ancient C flux was dominated by diffusive  $\text{CO}_2$  emissions ( $0.10 \pm 0.01 \text{ Tg C-CO}_2 \text{ yr}^{-1}$ , or 99% of the total ancient C emissions (Table 1)). Ice-free  $\text{CH}_4$  ebullition was neither directly observed nor estimated in our study. However, if ice-free ebullition represented 79% of the total ice-free  $\text{CH}_4$  emissions (as observed in yedoma-thermokarst lakes<sup>2</sup>) and was sourced completely from ancient C, cumulative emissions of ancient C via  $\text{CO}_2$  diffusion would still exceed the  $\text{CH}_4$  emissions (diffusion plus the hypothetical ancient ice-free ebullition of  $0.02 \text{ Tg C-CH}_4 \text{ yr}^{-1}$ ) in our region by over a factor of four. Nevertheless, in this unlikely scenario the climate-warming potential of ancient C emissions as  $\text{CH}_4$  is far greater than that of  $\text{CO}_2$ , because  $\text{CH}_4$  is 30 times more effective as a net radiative forcer on a molecule-to-molecule basis and on a 100-year timescale<sup>41</sup>. Ancient C flux as  $\text{CH}_4$  would outweigh the global warming potential of observed ancient C emission via  $\text{CO}_2$  diffusion if ice-free  $\text{CH}_4$  ebullition comprised roughly 70% of the total diffusive  $\text{CH}_4$  emissions in our study lakes  $((5.0 \pm 0.8) \times 10^{-3} \text{ Tg C-CH}_4 \text{ yr}^{-1})$  and was purely sourced from ancient C. This finding emphasizes the need for climate feedback studies of permafrost C to distinguish  $\text{CH}_4$  from  $\text{CO}_2$  emissions and whether each gas is predominantly sourced from ancient or young C.

Our regional-scale assessment provides an important baseline dataset for monitoring the emission sources of  $\text{CH}_4$  and  $\text{CO}_2$  from the climate-sensitive North Slope lakes. It also demonstrates that lakes in Arctic Alaska currently emit  $\text{CH}_4$  and  $\text{CO}_2$  predominantly from C pools that cycle between the land and atmosphere on timescales of decades to four millennia, even in areas where the lakes are actively eroding into relatively C-rich Pleistocene permafrost. Consequently, the Alaskan Arctic lakes are important systems for processing and returning freshly fixed C back to the atmosphere. Future emissions of ancient C are likely to increase, but our work provides further evidence that they will be restricted to areas in which the combination of warming temperatures, ancient OC and thermokarst favour the development of new or expanding taliks and shorelines<sup>18,42</sup>. Finally, diffusive  $\text{CO}_2$  emissions from young C



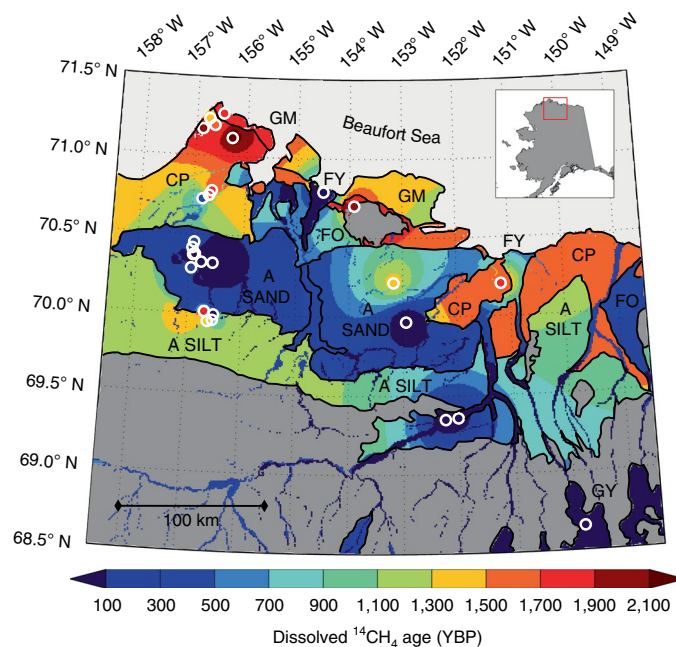


**Fig. 3 | Mean  $^{14}\text{C}$  age of dissolved  $\text{CH}_4$  in thaw lakes interpolated across Alaska's North Slope.** Circles indicate the location of 27 lakes measured for below-ice dissolved  $^{14}\text{CH}_4$  ( $n=1-2$  per lake). Methane ages were interpolated using inverse distance weighting with a  $1/20$  weight reduction parameter for predictions in non-similar geology categories (equations (9)–(11)), which gives the effect of pronounced geology boundaries. Major geological boundaries are also emphasized with black lines. Geological units: A. sand, aeolian sand; A. silt, aeolian silt; CP, coastal plain; FO, fluvial old; FY, fluvial young; GM, glaciomarine; GY, glacial young. Grey areas represent unobserved geological units. Methods and Supplementary Fig. 2 give an estimate for the quantitative uncertainty for this interpolation and Supplementary Fig. 1 depicts the lake distribution and geological units.

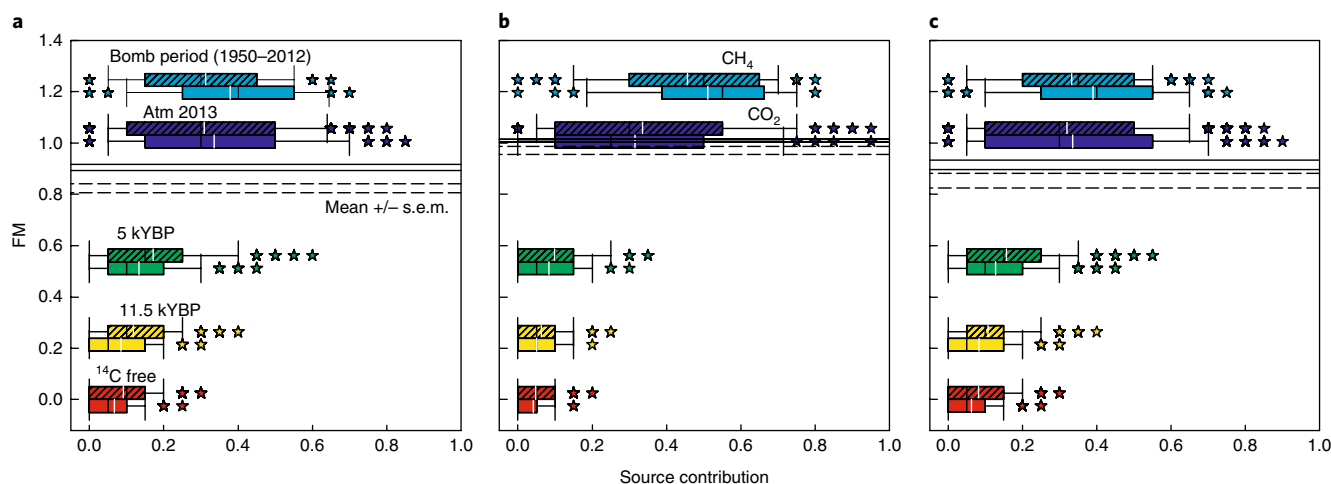


**Fig. 4 | Source apportionment of lake-dissolved  $\text{CH}_4$  and  $\text{CO}_2$  below ice.** Proportional source contributions to the mean  $^{14}\text{C}$  signature of dissolved  $\text{CH}_4$  are shown with hashed boxes, with open boxes for that of  $\text{CO}_2$ . **a**, Lake coastal plain geology ( $n$  lakes = 9,  $n$  mass-balance solutions = 411 ( $\text{CH}_4$ ) and 200 ( $\text{CO}_2$ )). **b**, Aeolian sand ( $n=9$ ,  $n=171$  and 46; sedimentary % OC =  $0.19 \pm 0.10$ ). **c**, Aeolian silt ( $n=3$ ,  $n=632$  and 295; sedimentary % OC =  $0.95 \pm 0.34$ ). The dashed and solid horizontal lines denote the  $\pm$  standard error range around the observed mean  $^{14}\text{C}$  values for  $\text{CH}_4$  and  $\text{CO}_2$  in each geological unit, respectively. The boxes show the mean (vertical white line), median, first and third quartiles, and the range of all the possible source contributions to the mean  $^{14}\text{C}$  value. Stars represent mass-balance solutions outside the 10th to 90th percentile range (whiskers), and are treated as outliers. The text and Methods describe the end members and mass-balance calculations. Atm, atmosphere.

sources currently account for nearly all (99%) of gaseous C loss from the North Slope lakes. Our multiyear regional lake survey concludes that future Arctic greenhouse-gas-emission research must consider the complexity of lake-forming processes, the variable geological settings of the entire circumpolar region and whether relatively fresh and young C or decomposing ancient permafrost C dominate the C cycling of Arctic lakes.

## Methods

Methods, including statements of data availability and any associated accession codes and references, are available at <https://doi.org/10.1038/s41558-017-0066-9>.

Received: 6 March 2017; Accepted: 20 December 2017;  
Published online: 29 January 2018

## References

1. Verpoorter, C., Kutser, T., Seekell, D. A. & Tranvik, L. J. A global inventory of lakes based on high-resolution satellite imagery. *Geophys. Res. Lett.* **41**, 6396–6402 (2014).
2. Wik, M., Varner, R. K., Anthony, K. W., MacIntyre, S. & Bastviken, D. Climate-sensitive northern lakes and ponds are critical components of methane release. *Nat. Geosci.* **9**, 99–106 (2016).
3. Kirschke, S. et al. Three decades of global methane sources and sinks. *Nat. Geosci.* **6**, 813–823 (2013).
4. Walter, K. M., Smith, L. C. & Chapin, F. S. Methane bubbling from northern lakes: present and future contributions to the global methane budget. *Phil. Trans. A.* **365**, 1657–1676 (2007).
5. Bastviken, D., Tranvik, L., Downing, J., Crill, P. & Enrich-Prast, A. Freshwater methane emissions offset the continental carbon sink. *Science* **331**, 50 (2011).
6. Tan, Z. & Zhuang, Q. Arctic lakes are continuous methane sources to the atmosphere under warming conditions. *Environ. Res. Lett.* **10**, 54016 (2015).
7. Schneider Von Deimling, T. et al. Observation-based modelling of permafrost carbon fluxes with accounting for deep carbon deposits and thermokarst activity. *Biogeosciences* **12**, 3469–3488 (2015).
8. Lawrence, D. M., Slater, A. G. & Swenson, S. C. Simulation of present-day and future permafrost and seasonally frozen ground conditions in CCSM4. *J. Clim.* **25**, 2207–2225 (2012).
9. Jorgenson, M. T. & Shur, Y. Evolution of lakes and basins in northern Alaska and discussion of the thaw lake cycle. *J. Geophys. Res. Earth Surf.* **112**, 1–12 (2007).
10. Strauss, J. et al. The deep permafrost carbon pool of the Yedoma region in Siberia and Alaska. *Geophys. Res. Lett.* **40**, 6165–6170 (2013).
11. Olefeldt, D. et al. Circumpolar distribution and carbon storage of thermokarst landscapes. *Nat. Commun.* **7**, 13043 (2016).
12. Matheus Carnevali, P. B. et al. Methane sources in Arctic thermokarst lake sediments on the North Slope of Alaska. *Geobiology* **13**, 181–197 (2015).
13. Bastviken, D., Cole, J., Pace, M. & Tranvik, L. Methane emissions from lakes: dependence of lake characteristics, two regional assessments, and a global estimate. *Glob. Biogeochem. Cycles* **18**, 1–12 (2004).
14. Schuur, E. A. G. et al. Climate change and the permafrost carbon feedback. *Nature* **520**, 171–179 (2015).
15. Arp, C. D. et al. Threshold sensitivity of shallow Arctic lakes and sublake permafrost to changing winter climate. *Geophys. Res. Lett.* **43**, 1–8 (2016).
16. Walter, K. M., Zimov, S. A., Chanton, J. P., Verbyla, D. & Chapin, F. S. Methane bubbling from Siberian thaw lakes as a positive feedback to climate warming. *Nature* **443**, 71–75 (2006).
17. Walter, K. M., Chanton, J. P., Chapin, F. S., Schuur, E. A. G. & Zimov, S. A. Methane production and bubble emissions from Arctic lakes: isotopic implications for source pathways and ages. *J. Geophys. Res.* **113**, G00A08 (2008).
18. Walter Anthony, K. et al. Methane emissions proportional to permafrost carbon thawed in Arctic lakes since the 1950s. *Nat. Geosci.* **9**, 679–682 (2016).
19. Zimov, S. A. et al. North Siberian lakes: a methane source fueled by pleistocene carbon. *Science* **277**, 800–802 (1997).
20. Brosius, L. S. et al. Using the deuterium isotope composition of permafrost meltwater to constrain thermokarst lake contributions to atmospheric CH<sub>4</sub> during the last deglaciation. *J. Geophys. Res.* **117**, G01022 (2012).
21. Bouchard, F. et al. Modern to millennium-old greenhouse gases emitted from ponds and lakes of the Eastern Canadian Arctic (Bylot Island, Nunavut). *Biogeosciences* **12**, 7279–7298 (2015).
22. Sepulveda-Jauregui, A., Walter Anthony, K. M., Martinez-Cruz, K., Greene, S. & Thalasso, F. Methane and carbon dioxide emissions from 40 lakes along a north–south latitudinal transect in Alaska. *Biogeosciences* **12**, 3197–3223 (2015).
23. Lindgren, P. R., Grosse, G., Anthony, K. M. W. & Meyer, F. J. Detection and spatiotemporal analysis of methane ebullition on thermokarst lake ice using high-resolution optical aerial imagery. *Biogeosciences* **13**, 27–44 (2016).
24. Wik, M., Thornton, B. F., Bastviken, D., Uhlback, J. & Crill, P. M. Biased sampling of methane release from northern lakes: a problem for extrapolation. *Geophys. Res. Lett.* **43**, 1256–1262 (2016).
25. Matveev, A., Laurion, I., Deshpande, B. N., Bhiri, N. & Vincent, W. F. High methane emissions from thermokarst lakes in subarctic peatlands. *Limnol. Oceanogr.* **61**, S150–S164 (2016).
26. Tranvik, L. J. et al. Lakes and reservoirs as regulators of carbon cycling and climate. *Limnol. Oceanogr.* **54**, 2298–2314 (2009).
27. Kling, G., Kipphut, G. & Miller, M. The flux of CO<sub>2</sub> and CH<sub>4</sub> from lakes and rivers in arctic Alaska. *Hydrobiologia* **240**, 23–36 (1992).
28. Negandhi, K. et al. Small thaw ponds: an unaccounted source of methane in the Canadian High Arctic. *PLoS ONE* **8**, e78204 (2013).
29. Frohn, R. C., Hinkel, K. M. & Eisner, W. R. Satellite remote sensing classification of thaw lakes and drained thaw lake basins on the North Slope of Alaska. *Remote Sens. Environ.* **97**, 116–126 (2005).
30. Hugelius, G. et al. Estimated stocks of circumpolar permafrost carbon with quantified uncertainty ranges and identified data gaps. *Biogeosciences* **11**, 6573–6593 (2014).
31. Schirrmeister, L., Froese, D., Tumskey, V., Grosse, G. & Wetterich, S. Yedoma: Late Pleistocene ice-rich syngenetic permafrost of Beringia. *Encycl. Quat. Sci.* **3**, 542–552 (2013).
32. Black, R. F. *Gubik Formation of Quaternary Age in Northern Alaska* Professional Paper 302-C (USGS, 1964).
33. Carter, L. D. A Pleistocene sand sea on the Alaskan Arctic Coastal Plain. *Science* **211**, 381–383 (1981).
34. Kanevskiy, M., Shur, Y., Fortier, D., Jorgenson, M. T. & Stephani, E. Cryostratigraphy of late Pleistocene syngenetic permafrost (yedoma) in northern Alaska, Itkillik River exposure. *Quat. Res.* **75**, 584–596 (2011).
35. Jorgenson, M. T. et al. *Permafrost Database Development, Characterization, and Mapping for Northern Alaska* Final Report (US Fish and Wildlife Service, 2014).
36. Greene, S., Walter Anthony, K. M., Archer, D., Sepulveda-Jauregui, A. & Martinez-Cruz, K. Modeling the impediment of methane ebullition bubbles by seasonal lake ice. *Biogeosciences* **11**, 6791–6811 (2014).
37. Phillips, D. L. & Gregg, J. W. Source partitioning using stable isotopes: coping with too many sources. *Oecologia* **136**, 261–269 (2003).
38. Townsend-Small, A., Akerstrom, F., Arp, C. & Hinkel, K. M. Spatial and temporal variation in methane concentrations, fluxes, and sources in lakes in Arctic Alaska. *J. Geophys. Res. Biogeosci.* **112**, 1–14 (2017).
39. Whittaker, M. J. Carbon and hydrogen isotope systematics of bacterial formation and oxidation of methane. *Chem. Geol.* **161**, 291–314 (1999).
40. Walter Anthony, K. M., Anthony, P., Grosse, G. & Chanton, J. Geologic methane seeps along boundaries of Arctic permafrost thaw and melting glaciers. *Nat. Geosci.* **5**, 419–426 (2012).
41. Myhre, G. et al. in *Climate Change 2013: The Physical Science Basis* (eds Stocker, T. F. et al.) 659–740 (IPPC, Cambridge Univ. Press, Cambridge, 2013).
42. Walter Anthony, K. M. et al. A shift of thermokarst lakes from carbon sources to sinks during the Holocene epoch. *Nature* **511**, 452–456 (2014).

## Acknowledgements

We are grateful to UIC Science (Ukpeagvik Inupiat Corporation) and the city of Atkasuk for logistical support and access to field sites, in particular A. Danner, N. Harcharek, E. Burnett, K. Newyear and D. Whiteman. We thank J. Chaplin (ChaplinAK Air) for flying and patiently floating. At UC Irvine, we thank M. Crawford, J. G. Mazariegos, M. A. Larios, M. Schweiger, C. McCormick, E. Ciraci and R. A. Jimenez for assistance with the equipment and/or sample or data processing, and the KCCAMS staff for assisting with isotope analysis. Funding was provided by the Hellman foundation, UCI Council on Research, Computing and Libraries (to C.I.C.), the ARCS foundation (to C.D.E.), and US National Science Foundation grants AON-1107607 (to K.H. and A.T.-S.) and ARC-1107481 (to C.D.A.). We thank D. H. Mann and P. Groves, who were instrumental in the sediment sampling. We also thank B. Jones and G. Grosse for their valuable assistance in the field.

## Author contributions

C.D.E., X.X., J.W., C.I.C., B.V.G. and J.W.P. performed the measurements. J.L.S. developed the methodology and produced the figures for the spatial CH<sub>4</sub> interpolations. C.D.E., C.I.C., K.M.H., A.T.-S., C.D.A. and B.V.G. were all involved with the field logistics and sampling. B.V.G. contributed to all the work and data related to the sedimentary organic C content sampling. All the authors participated in the interpretation and presentation of the results.

## Competing interests

The authors declare no competing financial interests.

## Additional information

**Supplementary information** is available for this paper at <https://doi.org/10.1038/s41558-017-0066-9>.

**Reprints and permissions information** is available at [www.nature.com/reprints](http://www.nature.com/reprints).

**Correspondence and requests for materials** should be addressed to C.D.E. or C.I.C.

**Publisher's note:** Springer Nature remains neutral with regard to jurisdictional claims in published maps and institutional affiliations.

## Methods

**Sample collection.** Water and dissolved-gas samples were collected from 40 lakes ( $\geq 0.27$  ha) on the North Slope of Alaska, USA (Supplementary Table 1). The lakes are part of the Circum-Arctic Lakes Observation Network (CALON, [www.arcticlakes.org](http://www.arcticlakes.org)). The CALON lakes are distributed along a 'western' and an 'eastern' transect that spans 150 and 300 km and is centred along the  $-156.5^\circ$  W and  $-151.9^\circ$  W parallels, respectively. On each transect, the lakes are divided into 3–8 clusters, which span local lake sizes<sup>43</sup>. Most lakes are shallow (mean 2.4 m, range 0.5–11.8 m) and probably well mixed. Along each transect, coastal lakes are characterized by cooler summer temperatures and a shorter ice-free period than lakes located further inland<sup>44</sup>.

For radiocarbon ( $^{14}\text{C}$ ) analyses of dissolved  $\text{CH}_4$  and  $\text{CO}_2$ , the lakes were sampled near their centres twice a year, with and without ice cover, in North Slope lake in 2013 and 2014. During the winter (April) of 2013 the CALON team collected water from below the ice from 19 lakes on the western transect and 17 lakes on the eastern transect, and in the winter (April) of 2014 from 23 lakes solely on the western transect. A hole 25 cm in diameter was drilled with an Eskimo auger (Shark Z51 (Eskimo)) and 1.3 l of water were collected without headspace into Nalgene square polyethylene terephthalate (PETE) media bottles with natural high density polyethylene screw caps (342040-1000 (Thermo Scientific)). As the sample froze, the bottles expanded to accommodate the volume change. Once thawed, the bottles regained their original shape. Samples were frozen in the field and kept frozen until further processing at the University of California (UC) Irvine.

During the summer, samples were collected in surface waters near the centre of each lake using a novel gas-extraction technique with a Liqui-Cel membrane contactor. Lake water was pumped ( $1.21 \text{ min}^{-1}$ ) for 60 min through a series of four particulate filters (178 and  $40 \mu\text{m}$  stainless-steel mesh filters T-29595-39 and T-2959-35 (Cole-Parmer), and  $20 \mu\text{m}$  and  $5 \mu\text{m}$  5" polypropylene sediment depth filters SD-25-0520 Flow-Pro and SD-25-0505 Hydronix (FreshWaterSystems)) and past a degassing membrane contactor (Liqui-Cel (Membrana)), in which bulk dissolved gases (including  $\text{N}_2$ ,  $\text{CH}_4$  and  $\text{CO}_2$ ) were collected in a pre-evacuated, pre-weighed 2 l stainless steel canister with a stainless steel bellows sealed valve (SS-4BG (Swagelok)). To prevent cross-contamination, all the filters were replaced and the system was flushed with lake water for 30 min prior to each sampling event. To prevent microbial activity, the whole system was flushed with dilute  $\text{H}_3\text{PO}_4$  acid for 10 min and then clean tap water for 15 min daily (after about four samples) and stored dry. This system eliminates the need to store and ship an average of 100 l of water for the extraction of  $\geq 0.1 \text{ mg C-CH}_4$ , or approximately 10 l for the same amount of C- $\text{CO}_2$  per sample for  $^{14}\text{C}$  analysis. At the same time and location, we measured water temperature and pH (PCD 650 (Oakton Instruments)).

During the summer of 2014, the lakes were also analysed for dissolved  $\text{CH}_4$  and  $\text{CO}_2$  concentrations. At the centre of each lake, three replicates of 20 ml of surface lake water were manually injected into capped (blue butyl rubber septa, CLS-4209-14 (Chemglass Life Sciences)) pre-evacuated 40 ml crimp-sealed glass vials over the course of 2 h. The vials were pre-loaded with  $20 \mu\text{l}$  of aqueous mercuric chloride to inhibit microbial activity.

**General surficial geological units.** The descriptions of each general geology unit defined in this work (coastal plain, aeolian sand, aeolian silt, fluvial old, fluvial young, glaciomarine, and glacial young) are already published<sup>35</sup>.

**Laboratory analyses. Radiocarbon analysis.** Dissolved gases were extracted from frozen water samples collected during the winter. One day prior to extraction, and when still frozen, the original screw caps on the sample bottles were replaced with septum caps (38–430 Microlink Open Top, Wheaton, custom 1/8" thick butyl rubber septa (McMaster-Carr)) in a pure  $\text{N}_2$  atmosphere. The sample was then left to thaw at room temperature overnight. Post-thaw, a 15% headspace was created with ultrapure  $\text{N}_2$  (NI UHP300 (Airgas)) in the bottle to produce the most-efficient  $\text{CH}_4$  extraction conditions for  $\text{CH}_4$  (ref. <sup>45</sup>) as dissolved  $\text{CH}_4$  is typically in lower abundance than  $\text{CO}_2$ . Dissolved gases were transferred to pre-evacuated, weighed 2 l stainless-steel canisters via headspace extraction.

Canisters that contained the winter and summer samples of dissolved gas were weighed to quantify the mass of dissolved gases collected and then balanced to 1 atm with ultrazero (C-free) air (AI UZ300 (Airgas)). The canister was then connected to a flow-through vacuum extraction line designed to extract sequentially  $\text{CH}_4$  and  $\text{CO}_2$  for  $^{14}\text{C}$  analysis<sup>46</sup>. As the sample gas is introduced to the vacuum line, (1)  $\text{CO}_2$  is frozen out in a liquid nitrogen (LN) trap, (2) carbon monoxide is converted into  $\text{CO}_2$  at  $290^\circ\text{C}$  and frozen out in a second LN trap and (3)  $\text{CH}_4$  is oxidized to  $\text{CO}_2$  in a  $975^\circ\text{C}$  furnace with cupric oxide pellets.  $\text{CH}_4$ -derived  $\text{CO}_2$  and sample  $\text{CO}_2$  were purified on the vacuum line, quantified manometrically and converted into graphite using the sealed-tube zinc-reduction method<sup>47</sup>. Isotopic standards were extracted using the same methods to evaluate the procedural contamination of the sampling methods extraction-line system (see below).

Alongside the procedural and analytical standards and  $^{14}\text{C}$ -free blanks, which represented all sampling and processing steps (see below), the graphite was measured for its  $^{14}\text{C}/^{12}\text{C}$  ratio with an accelerator mass spectrometer (AMS) at the W.M. Keck Carbon Cycle Accelerator Mass Spectrometer facility at UC Irvine<sup>48</sup> (equation (1) and Supplementary Table 2). For samples  $>0.2 \text{ mg C}$ , an aliquot of the

$\text{CH}_4$ -derived  $\text{CO}_2$  or the sample  $\text{CO}_2$  was analysed for  $\delta^{13}\text{C}$  with isotope-ratio mass spectrometry (IRMS) (GasBench II coupled to a Delta plus IRMS (Thermo Fisher Scientific) (Supplementary Table 2):

$$\left. \frac{^{14}\text{C}}{^{12}\text{C}} \right|_{\text{sample}, -25\text{‰}} = \left. \frac{^{14}\text{C}}{^{12}\text{C}} \right|_{\text{sample}} \left( \frac{1 + -25/1,000}{1 + \delta/1,000} \right)^2 \quad (1)$$

$$\text{FM} = \frac{\left. \frac{^{14}\text{C}}{^{12}\text{C}} \right|_{\text{sample}, -25\text{‰}}}{0.95 \left. \frac{^{14}\text{C}}{^{12}\text{C}} \right|_{\text{OX1}[-19\text{‰}]}} \quad (2)$$

Radiocarbon values are reported in FM, which is the  $^{14}\text{C}$  to  $^{12}\text{C}$  ratio in the sample relative to that of the oxalic acid-1 standard (OX1) (equation (2)). The measured sample ratio is normalized to a  $\delta^{13}\text{C}$  value of  $-25\text{‰}$  to correct for the mass-dependent fractionation of  $^{14}\text{C}$  (via measuring  $\delta^{13}\text{C}$  simultaneously in the AMS ( $\delta$  in equation (1)), divided by 0.95 times the activity of OX1 to normalize to the conventional pre-industrial wood standard in 1950, where the OX1 standard is corrected to its actual  $\delta^{13}\text{C}$  value of  $-19\text{‰}$  (ref. <sup>49</sup>).

Mean  $^{14}\text{C}$  ages reported in YBP (equation (3)), which represents a  $^{14}\text{C}$  age calculated from the averaged FM values from equation (2):

$$^{14}\text{C} \text{ age(YBP)} = -8,033 \ln(\text{FM}) \quad (3)$$

where 8,033 is the mean lifetime of  $^{14}\text{C}$ , in years, using the Libby half-life of 5,568 years. When calculating mean  $^{14}\text{C}$  ages, any FM values  $>1$  (indicative of samples that contain 'bomb  $^{14}\text{C}$ ' from post-1950 above-ground nuclear weapons testing) were replaced with 1 (calendar year 1950, FM of OX1) and then averaged across all the study lakes and within the general geology types.

We report  $^{14}\text{C}$  ages, as opposed to calibrated-calendar ages, because dissolved  $\text{CH}_4$  and  $\text{CO}_2$  represent an open system that exchanges with various other C pools with presumably different  $^{14}\text{C}$  ages within the lakes' C cycle. Calibrated-calendar ages only apply to C material in closed systems, in which the radioactive decay of  $^{14}\text{C}$  is the only flux term. In our case the  $^{14}\text{C}$  age serves as a tracer for the C source of the dissolved  $\text{CH}_4$  and  $\text{CO}_2$ .

**Validation of  $^{14}\text{C}$  results produced from the sampling methods.** As mentioned above, we developed two methods for sampling dissolved  $\text{CH}_4$  and  $\text{CO}_2$  for C-isotope analysis in relatively high concentration below-ice waters (winter), and in low-concentration open waters (summer). To validate the isotopic data produced from these methods, we conducted laboratory tests to determine whether our methods introduced any measurement bias or extraneous C that would affect the true  $^{14}\text{C}$  and  $^{13}\text{C}$  signature of the sampled gases.

Tests of the winter method demonstrated minimal extraneous C and fractionation effects in both  $\text{CO}_2$  and  $\text{CH}_4$  for both  $^{14}\text{C}$  and  $^{13}\text{C}$ . The modern  $^{14}\text{C}$  blank was small and reproducible ( $\sim 1.5 \mu\text{g C}$  and  $2.5 \mu\text{g C}$  for  $\text{CH}_4$  and  $\text{CO}_2$ , respectively (Supplementary Fig. 3)). This represents just 0.02% of the average extraction yields for both dissolved  $\text{CH}_4$  and  $\text{CO}_2$  in the winter samples, and had a negligible effect on the measured values after the  $^{14}\text{C}$  extraneous-mass correction. Additionally, we saw no effect from using the Nalgene PETE bottles, as their  $^{14}\text{CH}_4$  results were indistinguishable from those produced from headspace extractions using glass bottles. Likewise, the replicates of modern-C biogas lab standards (assessment of  $^{14}\text{C}$ -free C contamination), regardless of the sample size, yielded results within the range of 20 measurements of the biogas standards directly injected and combusted on the extraction line (Supplementary Fig. 3). To test the potential fractionation of  $^{13}\text{C}$  in  $\text{CH}_4$  and  $\text{CO}_2$ , we also compared the  $^{13}\text{C}$  results from headspace extractions with those of direct injection and combustion. For the direct injection and combustion of  $\text{CH}_4$ , the  $\delta^{13}\text{C}$  value was  $-48.32 \pm 0.21\text{‰}$  ( $n=3$ ) compared with  $-48.37 \pm 0.07\text{‰}$  ( $n=8$ ) for the headspace extractions—a deviation comparable to the IRMS measurement error ( $\sim 0.02\text{‰}$ ). For the direct injection of  $\text{CO}_2$ , the  $\delta^{13}\text{C}$  value was  $-5.2 \pm 0.07\text{‰}$  ( $n=3$ ), comparable to  $-5.3 \pm 0.48\text{‰}$  ( $n=4$ ) for the headspace extractions, which is also negligible.

We also tested the potential extraneous  $^{14}\text{C}$ -free C contamination of the Liqui-Cel system (used for low-concentration open waters) (Supplementary Fig. 4). Similar systems using Liqui-Cel membranes have proved successful for minimal and reproducible  $^{14}\text{C}$  blanks in marine settings, in which much greater volumes of water are degassed<sup>50</sup>. A recirculation system was built in the lab such that approximately 2 l of ultrapure deionized water (brought to pH  $\approx 2$  with dilute  $\text{H}_3\text{PO}_4$ ) could be sparged with ultrahigh pressure (UHP)  $\text{N}_2$  and flushed through the system to remove all the ambient gases and dissolved inorganic carbon (DIC) prior to the injection of modern biogas gas standards ( $\text{CH}_4$  and  $\text{CO}_2$ ). Similar to flushing with sample water in the field, the recirculating system was flushed with the  $\text{N}_2$ -sparged acidified water for 30 min, prior to the extraction of dissolved gases. After the flushing period, gas standards were injected into the recirculating water stream via a septa port and extracted through the Liqui-Cel membrane for 1 h (same duration as in the field sampling). Supplementary Fig. 4 shows the results from four replications of varying size for  $\text{CH}_4$  and  $\text{CO}_2$  relative



to the consensus values for the respective biogas standards. We determined the consistent addition of extraneous  $^{14}\text{C}$ -free  $\text{CO}_2$  over 1 h to be  $25 \pm 7.5 \mu\text{g}$ , which is roughly 3% of the mean mass yield for open-water dissolved  $\text{CO}_2$  samples. For  $\text{CH}_4$ , we determined a smaller extraneous  $^{14}\text{C}$ -free C effect of  $2 \pm 1 \mu\text{g}$ , which corresponds to approximately 2% of the mean mass yields for open-water dissolved  $\text{CH}_4$  samples. We applied these mass corrections and associated errors to all  $^{14}\text{C}$  data produced from the Liqui-Cel system. As all  $^{14}\text{C}$  data are also normalized to  $\delta^{13}\text{C} = -25\text{‰}$  during the AMS measurement (see above), any potential mass-dependent fractionation of the Liqui-Cel system or other sample-processing steps is reconciled in the final measurement and irrelevant for reported  $^{14}\text{C}$  data.

Although we made considerable effort to mirror field sampling, the recirculation system in the lab does not replicate perfectly the open-system sampling in the field. During field sampling, water is not recirculated through the membrane and water filters, but is pumped out of the system and back into the lake, away from the intake. We believe this means our extraneous  $^{14}\text{C}$  mass correction is conservative and probably overestimated for both  $\text{CH}_4$  and  $\text{CO}_2$ .

**Regional mean  $^{14}\text{C}$  ages for dissolved  $\text{CH}_4$  and  $\text{CO}_2$  emissions.** We estimated the regional mean age of diffusive  $\text{CH}_4$  and  $\text{CO}_2$  (847 and 392 YBP, respectively) emissions using a lake-area-weighted mean. Specifically, the mean age for each gas in each geological unit was weighted by the proportional lake area in that unit to the total lake area.

**Dissolved-gas concentration analysis.** Methane and  $\text{CO}_2$  were analysed by flame-ionization detection using a Shimadzu GC-2014 gas chromatograph (Shimadzu) at the USGS Woods Hole Coastal and Marine Science Center. Prior to analysis, vials that contained the 20 ml water samples were brought to 1 atm by injecting UHP He through the vial septa. The vials were then overpressured slightly by the addition of 3.2 ml He-sparged, low-pH water. Reducing the pH to  $<2$  transferred all the DIC species to the headspace as  $\text{CO}_2$ . After a 2 h equilibration, 3.2 ml of the headspace was removed from the vial. Gas and water exchanges were achieved using Becton-Dickinson plastic syringes and 18-gauge needles (Becton, Dickinson and Co.) connected via a plastic three-way stopcock. The extracted headspace gas was injected into a  $22 \text{ ml min}^{-1}$  He carrier gas through a gas-sampling valve, and  $\text{CH}_4$  and  $\text{CO}_2$  were separated at  $80^\circ\text{C}$  on a 80/100 mesh HayeSep D (Hayes Separations) ( $5 \text{ m} \times 1/8$  outside diameter) packed column.  $\text{CO}_2$  was analysed as  $\text{CH}_4$  after its reduction with a methanizer. Concentrations of  $\text{CH}_4$  and  $\text{CO}_2$  were determined against Scott Gas certified gas standards (Air Liquide) that spanned the range of observed values. Headspace  $\text{CH}_4$  concentrations were converted into dissolved concentrations using a literature method<sup>31</sup>. Total DIC, or  $[\text{DIC}]_{\text{total}}$  measured in the headspace of the acidified samples, was converted into  $\text{pCO}_2$  (or  $\text{CO}_{2\text{aq}}$ ) for use in lake-air gas exchange calculations following the conventions of Stumm and Morgan<sup>52</sup>:

$$[\text{CO}_{2\text{aq}}] = \frac{[\text{DIC}]_{\text{Total}}}{1 + \left( \frac{K_1}{[\text{H}^+]} \right) + \left( K_1 \frac{K_2}{[\text{H}^+]^2} \right)} \quad (4)$$

here  $[\text{H}^+]$  is the hydrogen ion concentration based on lake pH and  $K_1$  and  $K_2$  are the lake-temperature-adjusted equilibrium constants for the dissociation of  $\text{H}_2\text{CO}_3$  and  $\text{HCO}_3^-$ , respectively.  $\text{CO}_{2\text{aq}}$  is used as  $C_w$  in equation (5).

**Sedimentary OC content.** A volumetric sampler ( $747 \text{ cm}^3$ ) was used to collect sediment from a stratigraphic section ( $69^\circ 51' 5.84'' \text{ N } 154^\circ 51' 48.26'' \text{ W}$ ) of aeolian sand and silt that is representative of the permafrost and talik deposits underlying the lakes in these respective surficial geology units of the North Slope. This frozen sediment was cleared on a near vertical face and allowed to thaw just before sampling. To analyse % OC, we first removed soil carbonates by soaking  $1 \text{ cm}^3$  of dry sediment in a 10% HCl mixture overnight. We assumed that this removed all carbonate because: (1) a visual inspection of the untreated sediments determined the majority of inorganic C to be calcite (removed by 10% HCl at room temperature) and (2) % OC in HCl-treated samples was strongly positively correlated with the root biomass in the same samples (which means non-pedogenic carbonate was not a factor). Samples were then centrifuged, decanted and rinsed with deionized water until to reach a pH of 5.5. Acidified sediment samples were then analysed for C content on a C:N analyser (TruSpec (LECO) by analysing the products of sample combustion at  $950^\circ\text{C}$  for  $\text{CO}_2$  and using an infrared  $\text{CO}_2$  detector at the Forest Soils Laboratory at the University of Alaska Fairbanks. We estimated the analytical precision as the s.d. of values based on two replicates of the National Institute of Standards and Technology Buffalo River Sediment standards per 40 samples. The total s.d. for all the standards was  $<0.02\%$  OC.

**Regional  $\text{CH}_4$  and  $\text{CO}_2$  lake-atmosphere diffusive flux.** The fluxes ( $F$ ) of dissolved  $\text{CH}_4$  and  $\text{CO}_2$  were calculated using a Fickian diffusion model:

$$F = k(C_w - C_a) \quad (5)$$

Where  $C_w$  is the concentration of either  $\text{CH}_4$  or  $\text{CO}_2$  in the water,  $C_a$  is the concentration of  $\text{CH}_4$  or  $\text{CO}_2$  in the surface water that is in equilibrium with the atmosphere and  $k$  is the water-to-air gas-exchange velocity. In an effort to constrain

the temporal variability, we collected three water samples for dissolved  $\text{CH}_4$  and  $\text{CO}_2$  concentrations over the course of approximately 2 h in the same location near the centre of each lake. In our flux calculation,  $C_w$  represents the mean of the three samples. Atmospheric background values of  $1.91 \text{ ppm}$  for  $\text{CH}_4$  and  $400 \text{ ppm}$  for  $\text{CO}_2$  were taken from the National Oceanic and Atmospheric Administration's Barrow, AK observatory Global Monitoring Division database, and used to calculate  $C_a$ . To determine  $k$ , we used the model of Cole and Caraco<sup>53</sup>, which empirically determined the relationship of  $k_{600}$  ( $\text{cm hr}^{-1}$ ) and wind speed at  $10 \text{ m}$  ( $U_{10}$  ( $\text{m s}^{-1}$ )) to be:

$$k_{600} = 2.07 + 0.215 U_{10}^{1.7} \quad (6)$$

Once  $k_{600}$  is known, it is converted to  $k$  via:

$$k = \frac{k_{600}}{(600 / \text{Sc})^{-0.5}} \quad (7)$$

Where Sc is the temperature-adjusted Schmidt number of either  $\text{CH}_4$  or  $\text{CO}_2$ .

We assumed that all the diffusive fluxes of  $\text{CH}_4$  and  $\text{CO}_2$  occurred between ice breakup in the spring and freeze-up in the fall. In August of 2014, a subset of seven lakes within the glaciomarine, coastal plain, aeolian sand and aeolian silt geology categories were sampled for dissolved  $\text{CH}_4$  and  $\text{CO}_2$  at the surface. Daily fluxes were estimated for each lake for every ice-free day in 2014. For each lake, the ice-free period was determined as the cumulative number of days starting from the day before rapid warming was observed (indicative of ice break-up) and ending on the last day where daily average water temperature was above freezing (on average 122 d for the whole study region). This was determined from hourly water-temperature observations obtained by CALON (NSF Award no. 1107607) buoy monitoring stations. The temperature data were downloaded from the NSF Arctic Data Center (<https://arcticdata.io/catalog/#data/page/0>). Daily average water temperatures and wind speeds were also used to calculate the average solubility and gas-exchange velocities ( $k$ ), respectively, for  $\text{CH}_4$  and  $\text{CO}_2$  during each day of the ice-free period. Historical daily average wind data for the ice-free period was downloaded for stations at Barrow, AK and Atkasuk, AK from the NOAA National Centers for Environmental Information web service (<http://www.ncdc.noaa.gov/>). Wind data from either Barrow or Atkasuk were used based on each lake's proximity to either weather station.

The August concentrations of  $\text{CH}_4$  and  $\text{CO}_2$ , along with the lake pH measured at the time of sample collection, were applied to all ice-free days during the summer of 2014. This assumption is probably a source of error in our flux estimate. During the August survey, one lake (BRW 100) was replicated in time (measurements one week apart) and two others (BRW 130 and RDC 310) were replicated spatially (approximately 1 km apart on the lake). In both scenarios, the mean of the replicate concentration measurements was prescribed in the whole-summer flux calculations.

Winter (April 2014) dissolved-gas concentrations were calculated during the headspace equilibration technique (described above), in which the entire equilibrated headspace was collected and  $\text{CH}_4$  and  $\text{CO}_2$  were purified. Yields of  $\text{CH}_4$  and  $\text{CO}_2$  were measured manometrically using a calibrated baratron, and then used to determine the concentration of each gas in the original headspace. Headspace concentrations were then used with Henry's Law to determine the dissolved-gas concentration in each sample. As below-ice concentrations of dissolved  $\text{CH}_4$  and  $\text{CO}_2$  were typically much higher than during the ice-free August survey, it is likely that excess gas was emitted during ice breakup in the spring. Ice growth probably reaches a maximum depth in April.

Water-volume reduction from ice growth could explain 10–100% of the increased below-ice concentrations of dissolved  $\text{CH}_4$  and  $\text{CO}_2$  when compared with the concentrations in August. This effect was considered when estimating the rapid equilibration of dissolved gas with the atmosphere during the ice breakup in the spring (ice-out flux) from each lake. To estimate ice-out fluxes, we applied a concentration effect (based on the maximum ice thickness and lake volume) to August  $\text{CH}_4$  and  $\text{CO}_2$  concentration measurements. We then subtracted this concentration from the actual measured concentration below the ice in April. The difference was considered to be the  $\text{CH}_4$  or  $\text{CO}_2$  accumulation from sediment production and emission into the water during the ice-cover season. The accumulated mass was then divided by the number of days of ice cover in between when the ice first appeared on each lake in the autumn and the day that the below-ice concentrations were measured. This value (grams per day) is an estimate of the integrated average accumulation rate below the ice. Next, this rate was multiplied by the total number of ice-cover days to estimate the total accumulation of  $\text{CH}_4$  and  $\text{CO}_2$  below the ice in each lake. As this accumulation is conceived to be the excess dissolved  $\text{CH}_4$  and  $\text{CO}_2$  above the assumed open-water steady-state concentration measured in August, we interpret it as the total diffusive ice-out flux.

Including the estimate of ice-out fluxes, our regional average daily ice-free diffusive  $\text{CH}_4$  flux was  $6.2 \pm 3.4 \text{ mg CH}_4 \text{ m}^{-2} \text{ d}^{-1}$ . This estimate is within the range of pan-Arctic diffusive emissions from tundra-thaw lakes (mean  $15.6 \text{ mg CH}_4 \text{ m}^{-2} \text{ d}^{-1}$ , range  $0.5\text{--}90.1 \text{ mg CH}_4 \text{ m}^{-2} \text{ d}^{-1}$ ,  $n = 23$ ) (ref. 2). Our ice-out  $\text{CH}_4$  fluxes ranged from 0 to 14% ( $n = 7$ ) of total ice-free  $\text{CH}_4$  diffusive flux, which is less than previous estimates from North Slope lakes<sup>54</sup>. The average daily ice-free diffusive  $\text{CH}_4$  flux

(excluding ice-out flux) was  $5.9 \pm 0.1 \text{ mg CH}_4 \text{ m}^{-2} \text{ d}^{-1}$ , and closely resembles the average of  $6.9 \text{ mg CH}_4 \text{ m}^{-2} \text{ d}^{-1}$  of an open-water diffusion-only flux previously observed using similar methods for North Slope lakes<sup>27</sup>. Our mean daily diffusive  $\text{CO}_2$  flux estimate of  $2,620 \pm 2,240 \text{ mg CO}_2 \text{ m}^{-2} \text{ d}^{-1}$  is on the high end of the range of  $\text{CO}_2$  fluxes reported by a previous study of 25 North Slope lakes<sup>55</sup>.

Our data represent a minimum estimate for the total annual  $\text{CH}_4$  fluxes from Alaskan Arctic thaw lakes because we did not include ice-free ebullition or ice-bubble-storage emissions<sup>36,56,57</sup>. However, by measuring the diffusive  $\text{CH}_4$  flux in the centre of the lakes, where the water/atmosphere gas exchange velocity is probably higher than on the lake margins, the whole-lake diffusive flux of  $\text{CH}_4$  and  $\text{CO}_2$  may be slightly overestimated<sup>58</sup>.

Daily fluxes of  $\text{CH}_4$  and  $\text{CO}_2$  were calculated for each lake's ice-free period. The values were totalled and added to each lake's respective ice-out flux. This total value was treated as the annual diffusive flux for each lake.

All the lakes were sources of C to the atmosphere (regional total,  $0.89 \pm 0.2 \text{ Tg C yr}^{-1}$  ( $\text{C} = \text{C-CO}_2 + \text{C-CH}_4$ )). At the time of the flux measurement, one thaw lake, underlain by glaciomarine geology, was a sink for atmospheric  $\text{CO}_2$  ( $-42.6 \pm 0.7 \text{ mg C-CO}_2 \text{ m}^{-2} \text{ d}^{-1}$ ). However, high  $\text{CH}_4$  emissions combined with the estimated ice-out flux of  $\text{CO}_2$  from this lake were enough to outweigh the observed C sink, even when the sink was extrapolated to the whole ice-free season (117 d). Overall, this lake was an annual  $\text{CO}_2$  and  $\text{CH}_4$  source to the atmosphere of  $1.39 \pm 0.04 \text{ Mg C-CO}_2 + \text{C-CH}_4$ . We assumed this behaviour was consistent with that of other thaw lakes in the glaciomarine category and applied fluxes accordingly when upscaling to the whole region.

A lake survey in 2014<sup>59</sup> estimated that approximately 85,000 lakes of area  $> 0.5 \text{ ha}$  exist north of  $68^\circ \text{N}$  in Alaska. Using an ArcGIS shapefile ( $10,660 \text{ km}^2$ ) generated from this report and geospatial analysis, we determined the total lake surface area within each geology category where  $^{14}\text{C}$  measurements were made. The total study area, including the land and lake area ( $231,157 \text{ km}^2$ ), was determined by summing the areas of all general geology units contained within the lake survey<sup>59</sup>. Annual areal fluxes were averaged for each geological unit surveyed during August 2014 (seven lakes within four geologic units). For the geological units not sampled in August (fluvial young, fluvial old and glacial young (14% of the total lake area in study)), annual diffusive fluxes were prescribed from observed units that had similar below-ice concentrations in April. For lakes within the observed geological units (81% of the total), the annual diffusive C- $\text{CH}_4$  and C- $\text{CO}_2$  fluxes were estimated by multiplying the average areal fluxes in each geological unit by its respective total lake area. For lakes outside the observed geological units (19% of the total), the mean of the areal fluxes from the observed units was multiplied by the total lake area in the unobserved geology. To estimate the total annual diffusive flux from the entire study region, fluxes from the observed and unobserved lakes were added and are shown in Table 1.

The total diffusive flux of  $\text{CH}_4$  and  $\text{CO}_2$  sourced from ancient C (fixed from the atmosphere  $\geq 11,500 \text{ YBP}$ ) was calculated by multiplying the mean fraction of the ancient C emissions (average of the possible contributions from 11.5 kYBP plus  $^{14}\text{C}$ -free end members in the isotopic mass-balance model) for each geological unit by its respective total C flux. This gave the total ancient C flux (g) as both dissolved  $\text{CH}_4$  and dissolved  $\text{CO}_2$  for all the lakes in each geological unit. Similar to the total flux (described above), an estimate of the ancient C flux from lakes in the unobserved geological units was determined by multiplying the mean of the fraction of the ancient C from observed units by the estimated total C- $\text{CH}_4$  and C- $\text{CO}_2$  fluxes from the lakes in unobserved geology. This value was added to the total ancient flux from the lakes in observed units, and then divided by the total C flux (modern + ancient (for  $\text{CH}_4$  and  $\text{CO}_2$ )) and is presented as the flux-weighted fraction of total  $\text{CH}_4$  and  $\text{CO}_2$  emissions sourced from ancient C (Table 1).

**Five-source isotopic mass-balance model.** IsoSource<sup>37</sup>, an open-source Visual Basic software, was used to compute the range of possible contributions from five prescribed sources ( $f_A, f_B, f_C, f_D$  and  $f_E$ ) to the mean FM value of dissolved  $\text{CH}_4$  and  $\text{CO}_2$  in each geology class:

$$\begin{aligned} \text{FM}_S &= f_{\text{AFM}_A} + f_{\text{BFM}_B} + f_{\text{CFM}_C} + f_{\text{DFM}_D} + f_{\text{EFM}_E} \\ 1 &= f_A + f_B + f_C + f_D + f_E \end{aligned} \quad (8)$$

where  $\text{FM}_S$  is the predicted solution to the mass-balance equation and  $f_A$  is the proportional source contribution from decaying C sequestered during the post-bomb period (1950–2012). For  $\text{FM}_A$ , we used the integrated annual average of atmospheric  $^{14}\text{CO}_2$  from 1950–2012 from the Hua et al.<sup>60</sup> atmospheric record and extended it with the Barrow NOAA observatory record from X. Xu (personal communication) to give  $\text{FM}_A = 1.2211$ . Similarly,  $f_B$  is the proportional source contribution from decaying organic material of recent photosynthesis (calendar year 2013 atmospheric  $\text{CO}_2$   $\text{FM}_B$  value = 1.0313) (also from the Barrow NOAA observatory (X. Xu, personal communication)),  $f_C$  represents the contribution from decaying 5,000 YBP organic C ( $\text{FM}_C = 0.5366$ ),  $f_D$  represents decaying 11,500 YBP C ( $\text{FM}_D = 0.2389$ ) and  $f_E$  represents  $^{14}\text{C}$ -free 'also known as dead' C sources ( $\text{FM}_E = 0$ ). As there are more than two unknowns in equation (8), which allows no unique solution, this model uses the principle of mass balance to compute iteratively multiple combinations of feasible source contributions in 5% increments ( $f_A, f_B, f_C, f_D$  and  $f_E$ ). A combination of source proportions is considered feasible

when the predicted solution ( $\text{FM}_S$ ) falls within the 'tolerance value' range of the observed mean FM for each geological unit. The 'tolerance value' is equal to the standard error of the observed mean FM value for each geology class. Proportional contributions that fall outside the 10th and 90th percentile range of all computed solutions for a given source were considered unlikely and treated as outliers.

**Geospatial extrapolation of  $\text{CH}_4$  ages.** In the simplest form of inverse distance weighting (Fig. 3), predictions are made at an unobserved location using a weighted sum of the observations, in which the weights are inversely proportional to the distance between the unobserved and observed locations. As the  $^{14}\text{CH}_4$  age observed at a given location is correlated with its geological substrate type, we also include a parameter that reduces the weights of observations with geology types different from that of the predicted location.

Taken together, we estimate the  $^{14}\text{CH}_4$  age,  $Z$ , at an unobserved location,  $x$ , with geology type,  $g$ , as a weighted sum of the  $K$   $^{14}\text{CH}_4$  age observations,  $Z_k$ , at locations,  $x_k$ , with geology type,  $g_k$ , as:

$$Z(x) = \sum_{k=1}^K w_k Z_k / \sum_{k=1}^K w_k \quad (9)$$

with weights,  $w_k$ :

$$w_k = |x - x_k|^{-\beta} / G \quad (10)$$

and

$$G = \begin{cases} 1 & \text{if } g = g_k \\ 20 & \text{if } g \neq g_k \end{cases} \quad (11)$$

We use a typical value of  $\beta = 2$ , to reduce sharp gradients in the interpolated product. The choice of  $G$  was somewhat arbitrary and was selected based on visual inspection of the final product. Predictions were made on a regular  $1 \times 1 \text{ km}$  grid over the study area bounded by  $68.24^\circ \text{N}$ – $71.66^\circ \text{N}$  and  $159.13^\circ \text{W}$ – $147.77^\circ \text{W}$ . We only retain predicted ages at a location if at least one observation has the same geology substrate type.

Although we cannot formally quantify the interpolation error for points without direct measurements, we can provide an estimate of the interpolation's prediction quality in terms of the pairwise distances from measured and predicted points. We define a quality of prediction ( $Q^p$ ) at each predicted point as the effective number of measurements at a distance of 50 km that went into its interpolation (equation (12) and Supplementary Fig. 2, Equation 12).

$$Q^p = 50^\beta \sum_{k=1}^K w_k^* \quad (12)$$

where  $w_k^*$  is calculated in the same as  $w_k$  in equation (10), but by forcing distances  $|x - x_k|$  to take a minimum of 25 km. If this minimum distance was not applied, the  $Q^p$  of the predicted points that are in very close proximity to the measured points is much less meaningful.

**Averaging and statistics.** Where applicable (age of  $\text{CH}_4$  versus  $\text{CO}_2$ , ANOVA geology versus age for  $\text{CH}_4$  and  $\text{CO}_2$ , geospatial interpolation of  $\text{CH}_4$ , end-member determination for isotopic mass balance for  $\text{CH}_4$  and  $\text{CO}_2$ , and summer 2014 spatial and temporal replicates), replicate samples (spatial or temporal) were averaged before the statistical tests were conducted. Supplementary Table 4 gives a detailed summary of the statistical results and analysis.

**Data availability.** Supplementary Information gives the relevant data that support the findings of this study but omits the atmospheric radiocarbon data (X. Xu, personal communication) used to extend the record published by Hua et al. (2013).

## References

20. Brosius, L. S. et al. Using the deuterium isotope composition of permafrost meltwater to constrain thermokarst lake contributions to atmospheric  $\text{CH}_4$  during the last deglaciation. *J. Geophys. Res.* **117**, G01022 (2012).
43. Hinkel, K. M. et al. Thermokarst lakes on the Arctic Coastal Plain of Alaska: spatial and temporal variability in summer water temperature. *Permafrost. Periglac.* **23**, 207–217 (2012).
44. Hinkel, K. M. et al. Thermokarst lakes on the Arctic Coastal Plain of Alaska: geomorphic controls on bathymetry. *Permafrost. Periglac.* **23**, 218–230 (2012).
45. Yamamoto, S., Alcauskas, J. B. & Crozier, T. E. Solubility of methane in distilled water and seawater. *J. Chem. Eng. Data* **21**, 78–80 (1976).
46. Pack, M. A., Xu, X., Lupascu, M., Kessler, J. D. & Czimczik, C. I. A rapid method for preparing low volume  $\text{CH}_4$  and  $\text{CO}_2$  gas samples for C-14 AMS analysis. *Org. Geochem.* **78**, 89–98 (2015).
47. Xu, X. et al. Modifying a sealed tube zinc reduction method for preparation of AMS graphite targets: reducing background and attaining high precision. *Nucl. Instrum. Methods Phys. Res. B* **259**, 320–329 (2007).
48. Beverly, R. K. et al. The Keck Carbon Cycle AMS Laboratory, University of California, Irvine: status report. *Radiocarbon*, **52**, 301–309 (2010).

49. Stuiver, M. & Polach, H. Reporting of  $^{14}\text{C}$  data. *Radiocarbon* **19**, 355–363 (1977).
50. Sparrow, K. J. & Kessler, J. D. Efficient collection and preparation of methane from low concentration waters for natural abundance radiocarbon analysis. *Limnol. Oceanogr. Methods* **15**, 601–617 (2017).
51. Magen, C. C. et al. A simple headspace equilibration method for measuring dissolved methane. *Limnol. Oceanogr. Methods* **12**, 637–650 (2014).
52. Stumm, W. & Morgan, J. J. *Aquatic Chemistry: Chemical Equilibria and Rates in Natural Waters* 3rd edn (Wiley, Chichester, 1995).
53. Cole, J. & Caraco, N. Atmospheric exchange of carbon dioxide in a low-wind oligotrophic lake measured by the addition of  $\text{SF}_6$ . *Limnol. Oceanogr.* **43**, 647–656 (1998).
54. Phelps, A., Peterson, K. & Jeffries, M. Methane efflux from high-latitude lakes during spring ice melt. *J. Geophys. Res.* **103**, 29029–29036 (1998).
55. Kling, G. W., Kipphut, G. W. & Miller, M. C. Arctic lakes and streams as gas conduits to the atmosphere: implications for tundra carbon budgets. *Science* **251**, 298–301 (1991).
56. Wik, M. et al. Energy input is primary controller of methane bubbling in subarctic lakes. *Geophys. Res. Lett.* **41**, 555–560 (2014).
57. Boereboom, T., Depoorter, M., Coppens, S. & Tison, J.-L. Gas properties of winter lake ice in Northern Sweden: implication for carbon gas release. *Biogeosciences* **9**, 827–838 (2012).
58. Schilder, J. et al. Spatial heterogeneity and lake morphology affect diffusive greenhouse gas emission estimates of lakes. *Geophys. Res. Lett.* **40**, 5752–5756 (2013).
59. Grunblatt, J. & Atwood, D. Mapping lakes for winter liquid water availability using SAR on the north slope of Alaska. *Int. J. Appl. Earth Obs. Geoinf.* **27**, 63–69 (2014).
60. Hua, Q., Barbetti, M. & Rakowski, A. Z. Atmospheric radiocarbon for the period 1950–2010. *Radiocarbon* **55**, 2059–2072 (2013).